Chinese Journal of Chemical Engineering 90 (2026) 361–371

Contents lists available at ScienceDirect

Chinese Journal of Chemical Engineering

journal homepage: www.elsevier.com/locate/CJChE

Full Length Article

Enhanced combustion and hydrophobic performance of aluminum micro-particles coated with high-energy fluorine-containing materials

Tingting Ma [1, #], Junjian Xie [2, #], Hui Li [3], Kaixin Wei [1], Zhibin Xu [1], Zihui Meng [1], Xiu-tian-feng E [1, *]

[1] School of Chemistry and Chemical Engineering, Beijing Institute of Technology, Beijing 100081, China
[2] School of Chemistry and Chemical Engineering, Northwestern Polytechnical University, Xi'an 710072, China
[3] Xi'an Modern Chemistry Research Institute, Xi'an 710065, China

ARTICLE INFO

Article history:
Received 15 June 2025
Received in revised form
22 August 2025
Accepted 16 September 2025
Available online 5 December 2025

Keywords:
Aluminum micro-particles
Fluorinated energetic small-molecule
Surface coating
Ignition
Combustion
Hydrophobicity

ABSTRACT

Fluorine-containing compounds have proven to be effective coating materials for enhancing the combustion efficiency of aluminum micro-particles (Al MPs). However, these compounds are usually low-energy polymeric materials, which may inevitably diminish the overall energy density of propellants or explosives. This study introduces a two-step coating strategy using fluorinated energetic small-molecule 2-NCF to coat Al MPs, employing $FeCl_3$ as an intermediate layer. Compared to pristine Al MPs, 2-NCF coated Al MPs can reduce the ignition delay from 36 ms to 3 ms and shorten the time to maximum flame area from 551 ms to 114 ms, accompanied by intensified sparking combustion. Thermal analyses demonstrate that the energetic 2-NCF induces localized micro-explosions to disrupt the alumina shell, and the fluorinated segments produced by 2-NCF react with the aluminum, followed by β-AlF_3 to α-AlF_3 phase evolution, which sustains oxygen penetration for complete aluminum core oxidation to release more energy. The 2-NCF coating concurrently enhances hydrophobicity of Al MPs, elevating contact angles from 0° to 120°. This coating can effectively block water penetration and prevent hydrolysis of the inner aluminum during long storage. This work demonstrates the potential of 2-NCF as an excellent high-energetic coating material to enhance the combustion and hydrophobic performance of aluminum powder.
© 2025 The Chemical Industry and Engineering Society of China, and Chemical Industry Press Co., Ltd. All rights are reserved, including those for text and data mining, AI training, and similar technologies.

1. Introduction

Aluminum powder, typically in micrometer-sized particles, has been widely used in the field of propellants and explosives [1–4], due to its excellent properties, such as high energy density [5–7], low oxygen consumption, outstanding energy release efficiency [8], and low cost. However, aluminum micro-particles (Al MPs) readily form a dense layer of aluminum oxide (Al_2O_3) on its surface, and its melting point (2072 °C) is significantly higher than that of aluminum (660 °C) [9,10]. This oxide layer hinders the further combustion and energy release of the Al MPs' interior, which results in an increased ignition temperature and exacerbates the agglomeration and two-phase flow phenomena, thereby reducing the specific impulse of propellants [11–14]. Furthermore, Al MPs are highly susceptible to reacting with water, leading to their deactivation, particularly when utilized in underwater weapons [15,16]. Consequently, achieving high combustion efficiency, lowering the ignition temperature, and enhancing the hydrophobicity of Al MPs are among the most critical research directions in the field of weapons with energetic materials.

An effective method to enhance the combustion and hydrophobic performance of Al MPs is to coat combustion-enhancing materials or waterproof materials on their surfaces. It has been reported that polymeric materials with high fluorine content, like PTFE [17–20], PVDF [21–23], and PFPE [24,25], can release highly oxidative HF gases, which effectively degrade the

* Corresponding author.
E-mail address: xtf_e@bit.edu.cn (X.-t.-f. E).
# These authors contributed equally to this work.

https://doi.org/10.1016/j.cjche.2025.09.035
1004-9541/© 2025 The Chemical Industry and Engineering Society of China, and Chemical Industry Press Co., Ltd. All rights are reserved, including those for text and data mining, AI training, and similar technologies.

aluminum oxide shell and form gaseous AlF_3 [26,27], improving the combustion efficiency of aluminum. Also, the exothermic reaction between aluminum and fluorine liberates energy of about 56.10 $kJ \cdot g^{-1}$, nearly doubling the 30.98 $kJ \cdot g^{-1}$ output observed in aluminum-oxygen combustion processes, thus releasing more energy [28]. Lots of effort has been devoted to coating the surface of Al MPs with fluoropolymers. For example, Hu *et al.* [29] employed the evaporation-induced self-assembly (EISA) method to coat polytetrafluoroethylene (PTFE) onto the surface of Al particles. Li *et al.* [30] constructed a polydopamine-fluorinated (PF) coating on Al surface through the covalent modification of polydopamine (PDA) with thiol-terminated organic fluorides. Wang *et al.* [31] synthesized a triblock copolymer (G-F-G) through the ring-opening addition reaction of glycidyl azide polymer (GAP) with 2,2'-(2,2,3,3,4,5,5-octafluorohexane-1,6-diyl) bis (oxirane) (fluoride), which firmly adhere to the surface of the Al powder. Huang *et al.* [9] developed a core-shell structured Al@(PFDTES/GAP) through hydrolysis of perfluorodecyltriethoxysilane (PFDTES) and co-reaction with glycidyl azide polymer (GAP) on aluminum powder surfaces. For enhancing the hydrophobicity of Al MPs, methods such as surface modification, nanocoating, and self-assembled monolayers can be employed [31–33]. These techniques reduce the contact between water molecules and Al MPs by forming a low surface energy protective film or introducing hydrophobic groups, thereby improving its hydrophobic properties [34,35]. However, those coating strategies typically involve more complex manufacturing processes. More critically, these polymer fluorocompounds generally lack energy content, and an excessive amount of those coating materials will inevitably reduce the overall energy density of propellants or explosives. Therefore, it is necessary to consider adopting an high-energetic coating material that can be applied to Al MPs through a relatively simple process, simultaneously enhancing their combustion and hydrophobic performance.

Herein, we developed a straightforward two-step method to coat the surface of Al MPs using a fluorine-containing energetic material, dinitro-5,5-bis(trifluoromethyl)hexahydroimidazo[4,5-d]imidazole-2(1H)-one (2-NCF), which possesses energetic functional groups, *i.e.* two nitrogen-rich heterocyclic rings and two nitro groups. Initially, $FeCl_3$ was applied to coat Al MPs as an intermediate layer, using single-solvent method. Then, 2-NCF was introduced to the surface of Al MPs forming a uniform coating layer. As a contrast, the characteristics of pristine Al MPs, 2-NCF coated Al MPs and their physical mixture samples were tested. Simultaneously, a laser combustion apparatus is utilized to confirm the improvement on ignition and combustion characteristics of Al MPs facilitated by 2-NCF. Preliminary investigations have also been conducted into the interfacial interaction between 2-NCF and the surface of Al MPs, as well as its combustion-promoting mechanism. Moreover, the contact angle measurement and the long-term water resistance experiment are conducted to evaluate the hydrophobic performance of coated Al MPs. This research provides a new strategy and fundamental data for enhancing the combustion and hydrophobic properties of Al MPs.

2. Materials and Methods

2.1. Materials

Al MPs (the particle size is 0.5–3.0 μm) was purchased from Aladdin Biochemical Technology Co., Ltd. (Shanghai, China). 2-NCF was synthesized by our laboratory (the detailed synthesis method and structural characterization data of 2-NCF are provided in the Supplementary Material, Fig. S1, as they are not the focus of this work, they will not be described in detail here). *N,N*-dimethylformamide (DMF, 99%) were purchased from Beijing Bailingwei Technology Co., Ltd. Ferric chloride (98%) was obtained from Anhui Senrise Technology Co., Ltd. All the materials were utilized as received, without any further purification.

2.2. Preparation of coated Al MPs

The synthesis of coated Al MPs is operated at room temperature, and the process is illustrated in Fig. 1. Under a nitrogen atmosphere, 0.1 g Al MPs was added to 50 ml DMF under sonication for 30 min, followed by mechanical stirring for 30 min. Then, 0.006 g ferric chloride was introduced into the above suspension. After stirring for 1 h, 2-NCF was added to the suspension. The mass ratio of Al MPs to 2-NCF was 6:1, 4:1 and 1:1, denoted as TO-1, TO-2, TO-3, respectively. After another 6 h stirring, the particles were recovered by phase separation and rotatory evaporation, and finally dried under vacuum at 60 °C for 12 h. Additionally, Al MPs and 2-NCF were ground and mixed in a mortar with a mass ratio of 1:1, and the mixture was named as TO-P.

2.3. Characterization of coated Al MPs

The scanning electron microscope (SEM, Zeiss GeminiSEM 360) and energy dispersive spectroscopy (EDS) images were obtained at room temperture with a working distance of 8.5 mm, and an acceleration voltage of 5 or 10 kV. All samples underwent Au sputtering treatment. Transmission electron microscope (TEM, JEOL JEM-2100 Plus) was utilized to examine the structure of the samples, operating at an accelerating voltage of 200 kV. X-ray photoelectron spectroscopy (XPS, Thermo Scientific ESCALAB 250Xi) was utilized to analyze the elements and their oxidation states on the surface of the material. Fourier transform infrared spectroscopy (FT-IR, Thermo IS5) and X-ray diffraction (XRD, Ultima IV) were employed to characterize the molecular and crystalline structure of the samples.

The thermal properties of the samples were analyzed using a simultaneous thermal analysis (TG-DSC, Mettler-Toledo TGA/DSC^{3+}) across a temperature range of 40–1100 °C, with a heating rate of 20 °C·min^{-1} in an air atmosphere. The samples were contained in aluminum oxide crucibles. The ignition of the samples were conducted on the homemade ignition system, as shown in Fig. S2. The system mainly consists of a laser ignition device, a high-speed camera, and a synchronous signal generator. At room temperature and 1 atm (1 atm = 101.325 kPa), the combustion of each sample (0.5 g) was carried out in the combustion chamber with highly transmissive and temperature-resistant quartz glass. The laser beam is converged by 20 × micro-scope objective (Olympus, Tokyo, Japan), finally entrance vertically into the chamber to ignite the particles. The ignition laser power was 34 W. A high-speed camera (Phantom VEO E310L) captures images of flame propagation at a rate of 2500 frames per second, spanning the entire process from ignition to the completion of combustion. Each ignition event is triggered simultaneously by the synchronous signal generator, activating both the ignition device and the high-speed camera for imaging, thereby ensuring the accuracy of the experimental process. The hydrophobic performance of the samples was tested using the OCA15EC contact angle goniometer. The long-term water resistance experiment was conducted by placing 0.5 g samples in 1 cm-diameter glass weighing bottles. The bottles were then stored in environments with different relatively humidity levels (RH) for two weeks. After this period, the samples were retrieved and characterized.

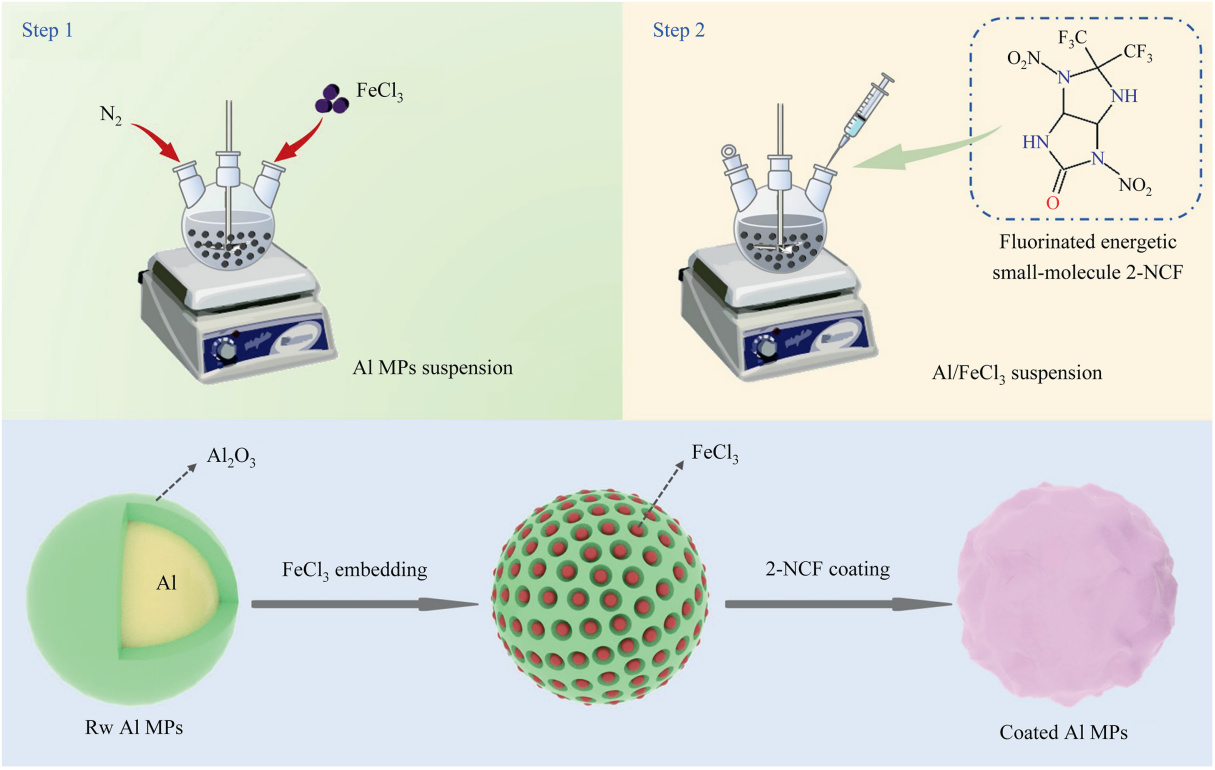

Fig. 1. The synthesis process of coated Al MPs.

3. Results and Discussion

3.1. Structure characteristics and interfacial interaction

Fig. 2 shows XRD patterns of pristine Al MPs, 2-NCF coated Al MPs and their physical mixture samples. The diffraction peaks for all samples align with the characteristic diffraction peaks of the metallic Al standard card (JCPDS No. 04-0787). Peaks observed at 38.4°, 44.9°, 65.2°, 78.2°, and 82.5° correspond to the (1 1 1), (2 0 0), (2 2 0), (3 1 1), and (2 2 2) crystal planes of Al, respectively. These results suggest that 2-NCF only coats the surface of MPs and has no effect on the bulk crystal phase. Moreover, there are some peaks observed within the range of 10° to 35° in both the 2-NCF coated Al MPs and their physical mixture samples, attributed to the characteristic diffraction peaks of 2-NCF.

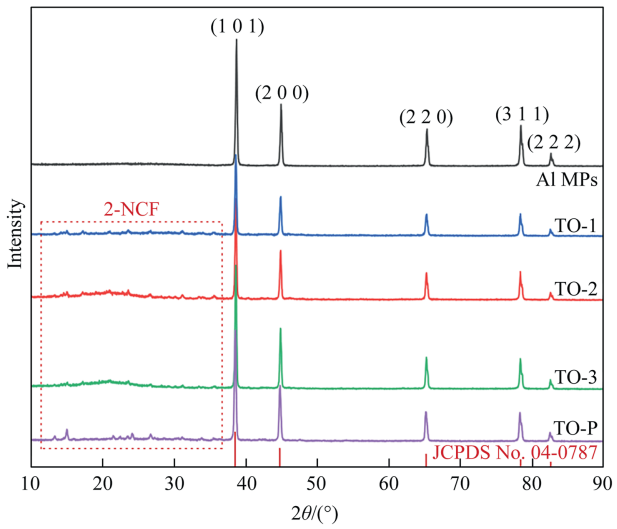

Fig. 2. XRD images of pristine Al MPs, 2-NCF coated Al MPs and their physical mixture samples.

SEM-EDS and TEM images in Fig. 3 show the size and surface appearance of pristine Al MPs and coated Al MPs. As show in Fig. 3(a), the pristine Al MPs exhibit a smooth surface with a size distribution of 0.5–3 μm, determined through particle size analysis using Image J software based on statistical measurements of at least 300 particles in the SEM image and there is *ca.* 4.2 nm thickness layer of Al_2O_3 on its surface (Fig. 3(g)). After being coated with varying amounts of 2-NCF, the surfaces of Al MPs exhibit different characteristics. When the coating amount of 2-NCF is relatively low (TO-1), the coating is non-uniform (Fig. 3(b)). Conversely, an excessive coating amount (TO-3) results in a relatively rough and uneven particle surface (Fig. 3(d)). When the coating amount of 2-NCF is appropriate (TO-2), a relatively uniform deposition layer is formed on the surface of the Al MPs (Fig. 3(c)). TEM image (Fig. 3(h)–(j)) shows that the borderline of coated MPs is not so clear due to the existence of organic layer, and the presence of C, N, O, and F elements in the EDS test confirmed that the coating layer was composed of 2-NCF, while the Fe element originated from $FeCl_3$ (Fig. 3(f)), an intermediate coating used during the preparation process. It has been reported that the Al_2O_3 shell can be partially corroded by $FeCl_3$ [36], resulting in the formation of small cavities on its surface (as observed in Fig. S3). Then, $FeCl_3$ would become lodged within these cavities [36]. The nitrogen atoms in 2-NCF, which possess lone pair electrons, can form coordination bonds with Fe^{3+}, thereby facilitating 2-NCF uniform deposition onto the surface of the Al MPs [37,38]. In contrast, for physically mixed sample, 2-NCF was merely dispersed in the interstices between the Al MPs or adhered sparsely to the surface of the Al MPs, without forming a uniform coating on their surfaces (Fig. 3(e)).

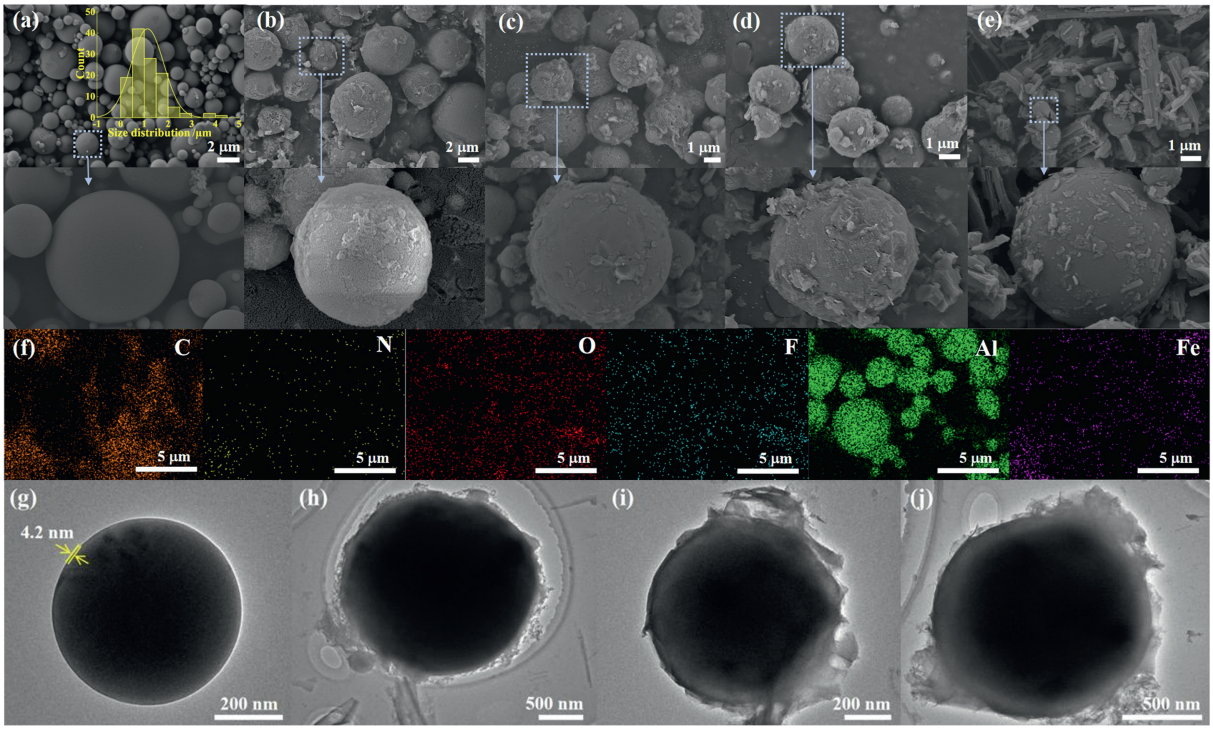

Fig. 3. SEM images of (a) pristine Al MPs, (b) TO-1, (c) TO-2, (d) TO-3, (e) TO-P, and (f) EDS images of TO-3. TEM image of (g) pristine Al MPs, (h) TO-1, (i) TO-2, and (j) TO-3.

IR spectra and XPS characterization were used to further detect the bonding between 2-NCF and Al MPs. As shown in Fig. 4(a), the N—H stretching vibration (3410 cm^{-1}), N—H flexural vibration (650–750 cm^{-1}) peaks of coated Al NPs are obviously weakened compared with pure 2-NCF, suggesting the N—H groups may interact with Al atoms. Meanwhile, three samples with different ratios (TO-1, TO-2, TO-3) all exhibited characteristic peaks near 1612 cm^{-1}, attributed to the N-NO_2 stretching vibration of 2-NCF, further confirming the presence of 2-NCF. The XPS spectra depicted in Fig. 4(b) reveal the presence of additional N 1s, F 1s, and Fe 2p peaks in both the coated Al MPs and the physical mixture samples, attributable to the existence of 2-NCF and $FeCl_3$. Furthermore, the C—F peak at 293.5 eV, which corresponds to the —CF_3 groups of 2-NCF in both TO-3 and TO-P (as shown in Fig. 4(c)), also supports this observation. Explanatorily, the C—C peak at 284.6 eV and the C=O peak at 288.0 eV in the C 1s spectra of the Al MPs originate from carbon present in the atmosphere. Obviously, the peak intensities of Al 2s and Al 2p in coated Al MPs and physical mixture samples are weakened compared with pristine Al MPs (Fig. 4(b)), which may be attributed to the coverage of the Al MPs surface by 2-NCF and $FeCl_3$. The binding energy shifts observed in the Al 2p region likely originate from steric effects induced by the dinitro groups in 2-NCF (Fig. 4(d)). In the N 1s region, no N 1s peaks are observable in Al MPs, whereas distinct peaks appear at 401.4 eV and 407.7 eV in both TO-3 and TO-P, which are attributed to the C—N bond and —NO_2 groups of 2-NCF, respectively (Fig. 4(e)). Notably, in the coated Al MPs, there exists a peak at 399.4 eV that is absent in TO-P, and this peak may be assigned to Fe-N[37]. It can be inferred that when 2-NCF is present in the solvent, the H atom of its N—H group becomes relatively reactive and tends to detach, leaving the N atom negatively charged with a lone pair of electrons. As a Lewis base, this negatively charged N atom then forms an N—Fe covalent bond with $FeCl_3$ which acts as a Lewis acid.

3.2. Thermal decomposition and energy release process

TG analysis was conducted to quantify the amount of 2-NCF chelated on the surface of Al MPs and to assess the thermal decomposition process of all samples in an air atmosphere. As shown in Fig. 5(a), pristine Al MPs exhibit no weight change before 600 °C due to the hindrance effect of the surface alumina layer [38]. In contrast, the weight changes of the other four samples containing 2-NCF primarily undergo four stages. The slight weight loss before 200 °C originate from the evaporation of residual solvents. Subsequently, a significant mass loss begins around 200 °C, primarily attributed to the decomposition of 2-NCF (2-NCF decomposes almost completely at around 200 °C, as shown in Fig. S4), corresponding to the exothermic peak at about 200 °C in the DSC curve (Fig. 5(b), Fig. S5). The mass loss for TO-1, TO-2, TO-3, and the physical mixture is 14.3%, 18.6%, 47.2%, and 51.8%, respectively, which aligns with the amount of 2-NCF added.

Similar to pristine Al MPs, all samples exhibit two stages of mass increase at 625–680 °C and 800–1100 °C (Fig. 5(a)). The weight gain of pristine Al MPs at 625 °C may relate to phase change of alumina layer, during which a small amount of aluminum undergoes an oxidation reaction [39]. Other samples also exhibit similar phenomena within this temperature range, as verified by the exothermic peak in the DSC curve (Fig. 5(b)). A slight mass increase is then observed before 700 °C, which is attributed to the melting, and this melting process is also accompanied by an endothermic peak (660 °C) in the DSC curve (Fig. 5(b)). As the temperature continued to rise, the continued mass increase of the samples is mainly due to the oxidation of aluminum [40]. In the final stage, pristine Al MPs begin to gain mass from 800 °C, with a total mass increase of 63.1% by 1100 °C. The trend in mass increase for the physical mixture is similar to pristine Al MPs, with a total mass increase of 20.7% by 1100 °C. However, the coated Al MPs (TO-1, TO-2, and TO-3) begin to gain

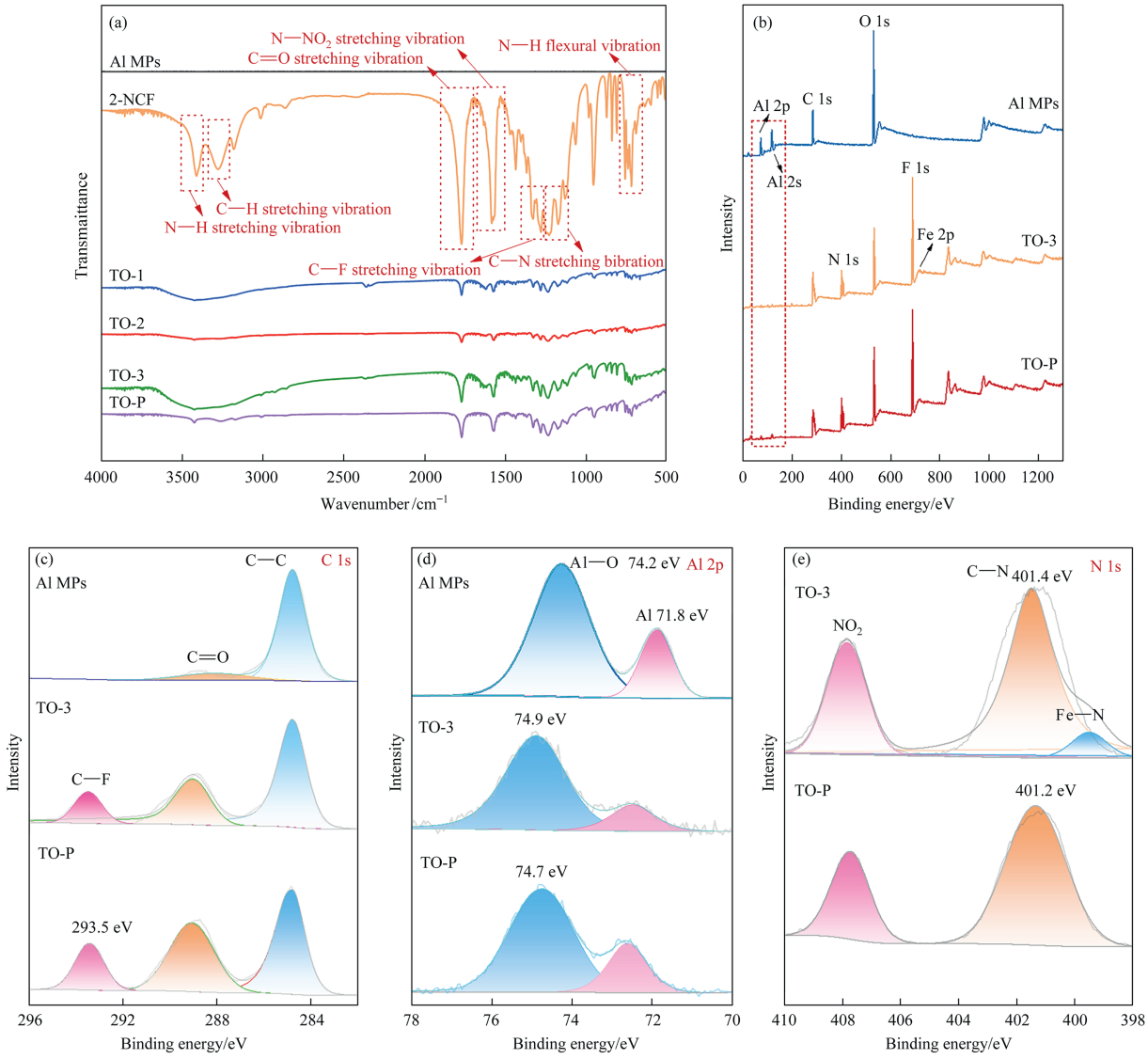

Fig. 4. (a) FT-IR spectra, (b) XPS spectra and (c)-(e) binding energy of different samples.

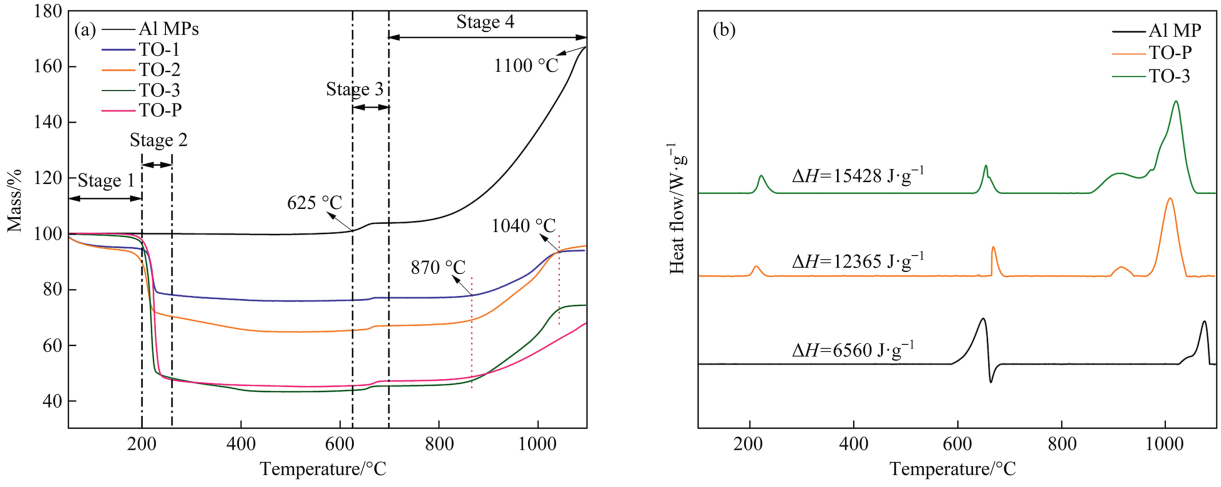

Fig. 5. (a) TG and (b) DSC curves of pristine Al MPs, 2-NCF coated Al MPs and their physical mixture samples.

mass near 900 °C and cease gaining mass at 1040 °C, indicating that the reaction of Al MPs has ended at this point. It has been reported that the inert aluminum oxide layer on the surface of Al MPs can react with fluorine-containing materials to form β-AlF_3 [25,28,40,41]. Therefore, it is inferred that after the decomposition of 2-NCF, the exposed aluminum may react with the generated F to form β-AlF_3, which coats the surface of Al MPs and isolates it from oxygen, resulting in a delay in the initial temperature of mass increase for the coated Al MPs samples from 800 °C for pristine Al MPs to nearly 900 °C. As the temperature further increases, β-AlF_3 transforms into α-AlF_3 [43,44], exposing the Al core to the atmosphere and triggering a vigorous oxidation reaction. It is evident that the heat flow release of coated Al MPs is also significantly greater than that of pristine Al MPs in the DSC curve at 800–1100 °C (Fig. 5(b)). Notably, the mass gain of the three coated Al MPs samples gradually increased with the increasing amount of 2-NCF, specifically 16.2%, 26.7%, and 28.1%. Due to the complete reaction of aluminum and the sublimation of AlF_3 43[45], the mass gain of the coated Al MPs samples are significantly lower than that of pristine Al MPs.

3.3. Ignition and combustion properties

A diode laser ignition experiment is conducted to evaluate the ignition and combustion property of different samples. The combustion process images are simultaneously recorded by a high-speed camera, as presented in Fig. 6. The time $t = 0$ ms in this experiment is defined as the instant when the camera captures the first frame after laser irradiation, and the ignition delay (ID) time is defined as the time interval between $t = 0$ ms and the first appearance of flame, which means the ignition process is ended and the combustion process begins. Fig. 6(a) shows the initial flame ignition of pristine Al MPs at 36 ms, subsequently followed by a weak yet sustained combustion process lasting about 500 ms, which indicates that the combustion process of Al MPs is sluggish and incompletely reactive. At around 593 ms, the most prominent flame is recorded, which persists until 666 ms. Evidently, as shown in Fig. 6(b)–(e), after coating 2-NCF onto the surface of Al MPs, the combustion flame of coated Al MPs becomes more intense and luminous. Furthermore, the coated Al MPs exhibit a notably more vigorous combustion process in comparison to the physical mixture. For instance, the combustion flame of TO-2 exhibits a particularly intense and jet-like appearance, accompanied by numerous sparks at 82 ms. This phenomenon is most likely attributable to the decomposition of 2-NCF, which generates a substantial amount of gas (Fig. S6), causing Al MPs in the combustion process to splatter. Subsequently, the flame undergoes a process of diminishing and then intensifying, reaching its maximum flame area at 409 ms. This phenomenon echoes the previous DSC analysis results (Fig. 5), indicating that the dense β-AlF_3 layer formed on the surface of Al MPs temporarily hinders the oxidation reaction and energy release. As this layer transforms into a loose α-AlF_3, the Al MPs undergo secondary combustion, leading to a larger and more intense flame. The heat release values obtained *via* DSC integration also confirm that the combustion heat of 2-NCF coated Al MPs (15428 $J{\cdot}g^{-1}$) and their physical mixture (12365 $J{\cdot}g^{-1}$) is significantly higher than that of pristine Al MPs (6560 $J{\cdot}g^{-1}$) (Fig. 5(b)). Moreover, the ID time of Al MPs is significantly shortened by the addition of 2-NCF. As summarized in Fig. 7(a), the ID times for TO-1, TO-2, TO-3, and TO-P are recorded at 18, 3, 16, and 30 ms, respectively. These represent reductions of 50%, 91.7%, 55.5%, and 16.7% compared to pristine Al MPs (36 ms). When the coating amount of 2-NCF is either too high or too low, its own combustion and decomposition require time, or the gas generation volume is relatively small, both of which will result in a comparatively longer ignition time for the coated aluminum powder. When the 2-NCF coating amount is appropriate (TO-2), the coating is more uniform and the ignition delay time is minimized. Additionally, the times taken for TO-1, TO-2, TO-3, and TO-P to reach their maximum flame areas (MFA) are

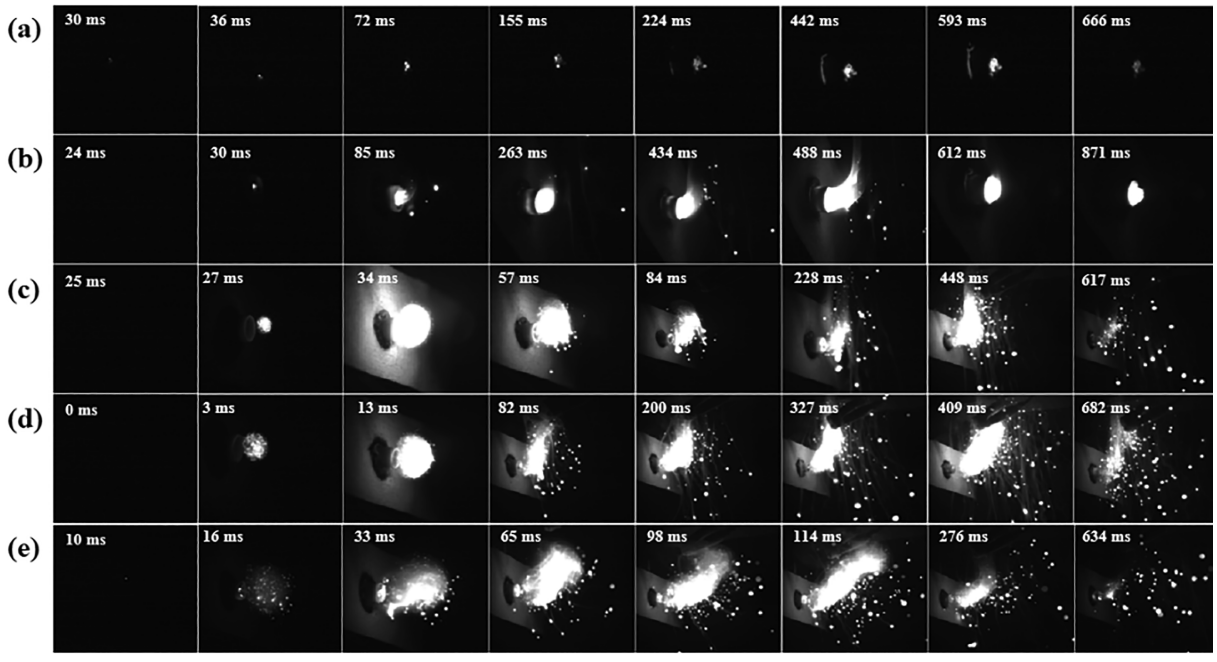

Fig. 6. Ignition and combustion images of (a) pristine Al MPs, (b) TO-P, (c) TO-1, (d) TO-2, and (e) TO-3.

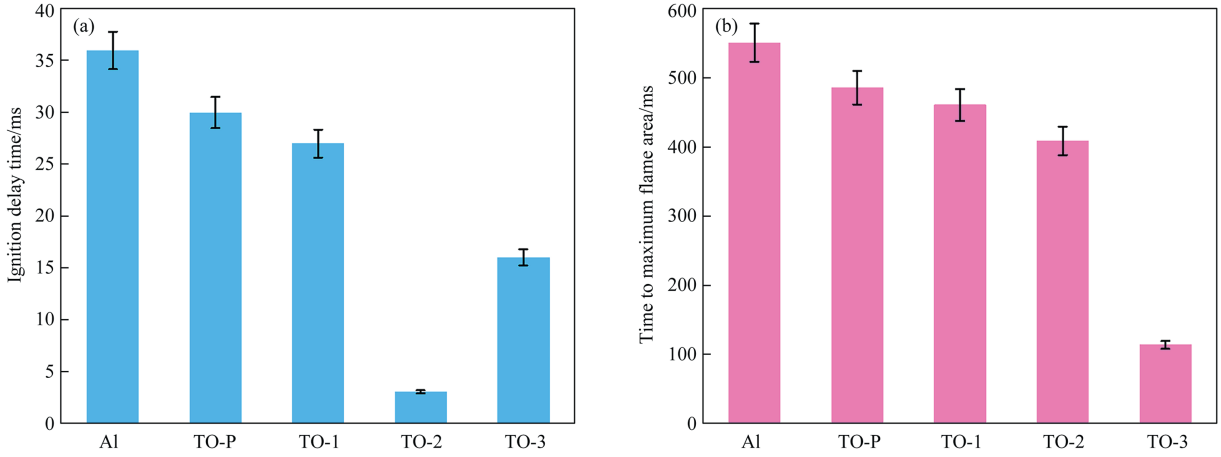

Fig. 7. The (a) ID time and (b) MFA time of different samples.

shortened to 461, 409, 114 and 486 ms, whereas this time is 551 ms for pristine Al MPs (Fig. 7(b)). Therefore, it is evident that 2-NCF has a positive impact on the combustion process of Al MPs.

Further, SEM images in Fig. 8 shows the morphology of the combustion residues. After combustion, a significant number of pristine Al MPs retain their intact spherical shapes, indicating that the alumina layer indeed hinder the reaction of the Al MPs, which corresponds to the faint combustion observed in Fig. 6(a). Among them, small area collapses are observed on the surface of some Al MPs due to the melting of Al at high temperatures (>650 °C). The stress generated by expansion caused cracks in the alumina shell, allowing the inner molten Al to react with air through the cracks. However, an oxide layer is quickly formed again, limiting the continued reaction of the Al MPs [46,47]. The XRD pattern also indicates that the pristine Al MPs are not fully reacted, and the main component of the residues remains Al (Fig. 8(f)). Notably, the combustion residues after adding 2-NCF exhibit many fragmented pieces or hollow spherical shells with obvious holes on their surface. Moreover, the combustion residues of coated Al MPs are more fragmented than those of their physical mixture (Fig. 8(b)–(e)), suggesting that the Al MPs burned more thoroughly after adding 2-NCF, which is confirmed by the characteristic peaks of alumina in the XRD (Fig. 8(f)). In particular, unlike the relatively smooth surfaces of the combustion residues of pristine Al MPs and physical mixtures, the surfaces of the coated Al MPs residues presented rough granular substances. Through XRD analysis (Fig. 8(f)), peaks corresponding to AlF_3 are detected among these substances, indicating that the HF and fluorinated fragments generated from the decomposition of 2-NCF (as illustrated in Fig. S6) have reacted with alumina. Since AlF_3 sublimates at 1277 °C (0.1 MPa), which is much lower than the combustion temperature (1715–2000 °C) of Al particles [45], so only part of AlF_3 still remains in the combustion residues, which is consistent with the findings of previous TG analyses.

Based on the above analysis of thermal decomposition and combustion processes, as well as relevant literature reports

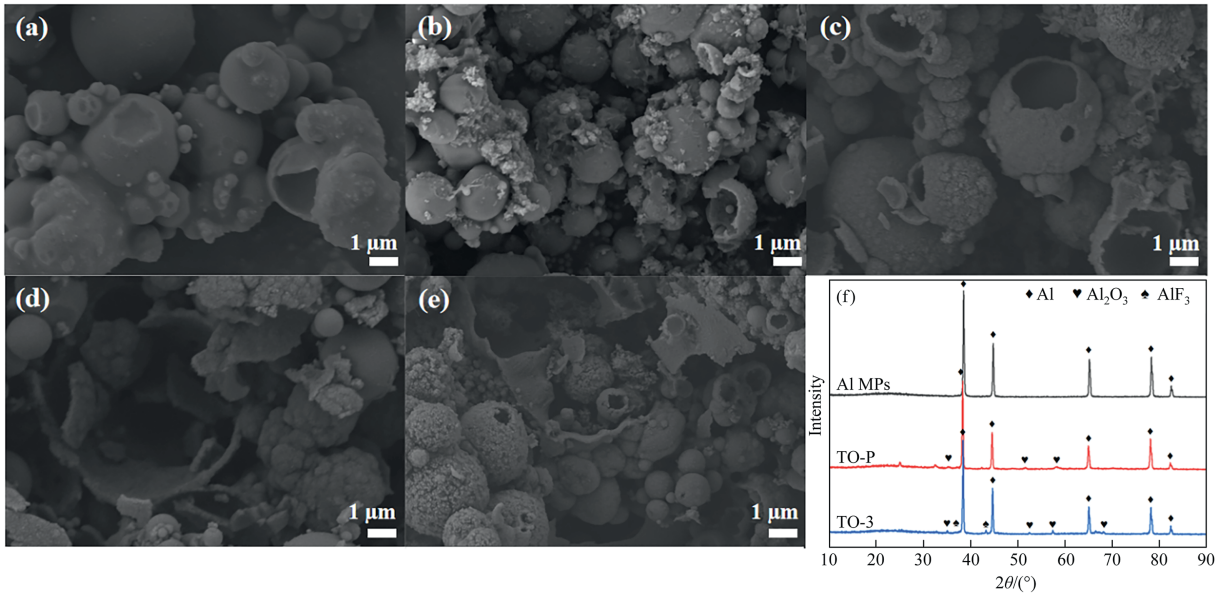

Fig. 8. SEM images of the combustion residues: (a) pristine Al MPs, (b) TO-P, (c) TO-1, (d) TO-2, (e) TO-3, and their (f) XRD patterns.

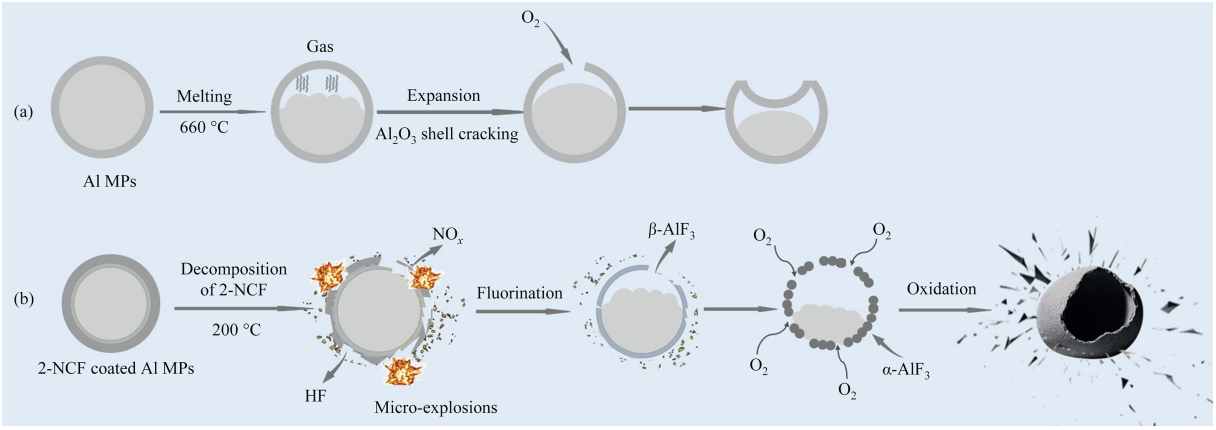

Fig. 9. Proposed combustion mechanism diagram of 2-NCF coated Al MPs.

[38–42], we propose a potential combustion mechanism for the 2-NCF coated Al MPs. As shown in Fig. 9, 2-NCF initially undergoes decomposition, yielding small molecular products such as NO_x, HF, and fluorinated segments (Fig. S6). These small molecules can disrupt the alumina layer on the particle surface and expose more inner aluminum for oxidation reactions. In the case of pristine Al MPs, the newly formed oxide layer would hinder further Al reaction. However, the HF and fluorinated segments produced by 2-

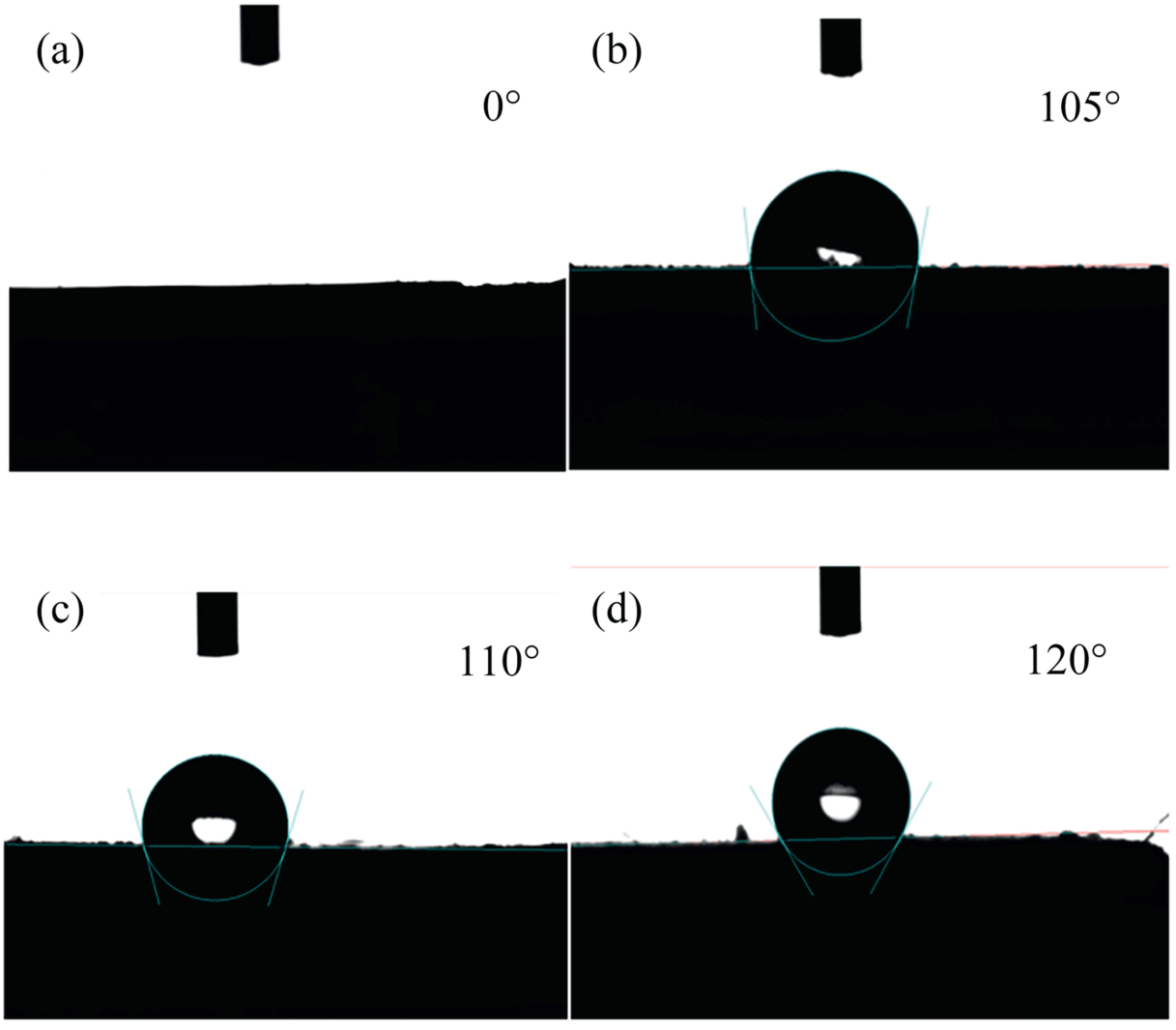

Fig. 10. Contact angle test images of (a) pristine Al MPs, (b) TO-1, (c) TO-2, and (d) TO-3.

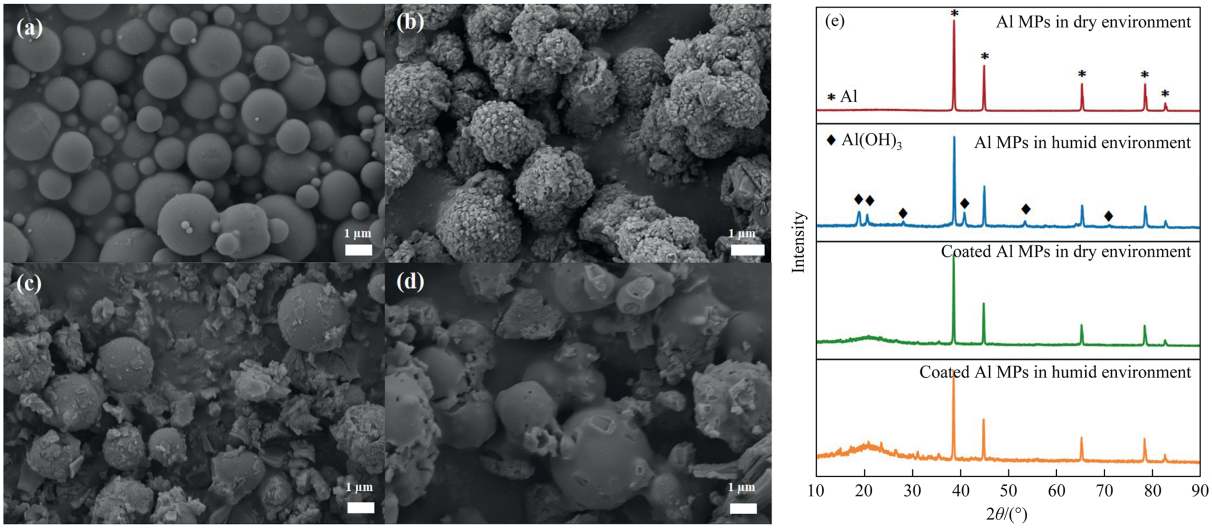

Fig. 11. SEM images of pristine Al MPs (a) in dry and (b) humid environment, 2-NCF coated Al MPs (c) in dry and (d) humid environment after two weeks, and their (e) XRD patterns.

NCF can react with the alumina to form a β-AlF_3 layer, which would transform into α-AlF_3 layer. Oxygen then permeates through the gaps in the α-AlF_3 layer to continue reacting with the inner Al, resulting in hollow spherical combustion residues. Simultaneously, the abundant gases generated cause the shell to fragment, producing numerous sparks during the combustion process. As more Al involved in the oxidation reaction, the combustion of 2-NCF coated Al MPs becomes more intense, releasing greater amount of energy.

3.4. Hydrophobic performance

The deactivation of Al MPs, particularly its reaction with water, is commonly encountered when stored in damp environments or utilized in underwater weaponry. The hydrophobicity level of 2-NCF coated Al MPs is measured in a contact angle goniometer. Generally, the contact angle $\theta = 90°$ between the solid-liquid interface acts as a boundary. When $\theta < 90°$, the solid surface demonstrates hydrophilicity, allowing the liquid to readily wet the solid, and smaller contact angles indicate improved wettability. Conversely, when $\theta > 90°$, the solid surface exhibits hydrophobicity, making it challenging for the liquid to wet the solid. As presented in Fig. 10(a), water droplets swiftly wet and permeate the surface of pristine Al MPs, resulting in a contact angle of 0°, indicating that the aluminum surface is in a fully hydrophilic state. However, the contact angles of 2-NCF coated Al MPs are all over 90°, which are 105°, 110°, and 120° for TO-1, TO-2 and TO-3, respectively (Fig. 10(b)–(d)). This suggests that 2-NCF coated Al MPs have excellent hydrophobicity. Studies have indicated that fluorine-containing groups, such as —CF_3 and —F, exhibit strong hydrophobic properties [48]. Furthermore, the unique rough surface of the coated Al MPs (as shown in Fig. 10(b)–(d)) minimizes the contact area between the solid and liquid interfaces. This results in the formation of an air layer between the water droplets and the material surface, thereby enhancing the hydrophobicity of the coated particles [49]. Thus, it can be concluded that coating Al MPs with 2-NCF can effectively enhance their hydrophobicity, thereby preventing aluminum from deactivation during storage or use.

A long-term water resistance experiment is conducted, during which samples are statically placed in two distinct environments: a dry environment (<10% RH) and a humid environment (80.2% ± 0.4% RH) at 60 °C. Fig. 11(a)–(d) present SEM images of the samples retrieved after two weeks. In the dry environment, both pristine Al MPs and 2-NCF coated Al MPs exhibit no significant morphological changes (Fig. 11(a)–(c)), and XRD analysis confirms that their primary composition remain aluminum (Fig. 11(e)). However, in the humid environment, the originally smooth surfaces of pristine Al MPs become rough and are covered with small particulate matter (Fig. 11(b)). XRD results reveal new diffraction peaks at $2\theta = 18.7°$ (020), 20.4° (110), 40.8° (200), and 53.4° (220), which matched the diffraction pattern of $Al_2O_3{\cdot}3H_2O$ (JCPDS #74-1119) (Fig. 11(e)). This indicates that hydrolysis occurred on the aluminum surface, forming $Al(OH)_3$. Notably, for the 2-NCF coated Al MPs exposed to prolonged humid conditions, the surface remains smooth but appears wet (Fig. 11(d)). XRD analysis further confirms that their primary composition is still aluminum (Fig. 11(e)). This phenomenon may be attributed to the 2-NCF coating, which absorbs moisture over time under humid conditions, resulting in a wet surface morphology. This layer effectively blocks water penetration and prevents hydrolysis of the inner aluminum.

4. Conclusions

In summary, the small-molecule fluorine-containing energetic material (2-NCF) is successfully coated onto the surface of Al MPs (0.5–3 μm) using $FeCl_3$ as an intermediate layer. The interfacial interaction mechanism of 2-NCF coating on Al MPs is investigated in detail through the use of SEM-EDS, TEM, FTIR, and XPS techniques. $FeCl_3$ initially etches the Al_2O_3 layer embedded on the surface of the Al MPs, and subsequently, 2-NCF adheres tightly and uniformly to the Al MPs surface through N-Fe chemical bonds. Then, TG analysis reveals that 2-NCF coated Al MPs undergo four stages: evaporation of residual solvents below 200 °C, decomposition of 2-NCF at *ca.* 200 °C, melting of Al MPs at 650–680 °C, fluorination and oxidation reaction of Al MPs at 800–1100 °C. To further explore the energy release process of 2-NCF coated Al MPs, a laser combustion test is conducted. The ignition delay time of the coated Al MPs is reduced to 3 ms, while the ignition delay times for pristine Al MPs and the physical mixture sample are 36 ms and 30 ms, respectively. Additionally, the MFA time of the coated Al MPs is also shortened from 551 ms to 114 ms. Moreover, the combustion process becomes more intense, generating numerous sparks. DSC and combustion residue analyses confirm that 2-NCF

enhances the oxidation reaction of Al MPs, and facilitates the release of more energy (the combustion heat of 2-NCF coated Al MPs (15428 $J{\cdot}g^{-1}$) than that of pristine Al MPs (6560 $J{\cdot}g^{-1}$). Based on the above results, the presumed combustion mechanism is that the small-molecule energetic material, the abundant gases generated from 2-NCF can disrupt the alumina layer on the particle surface and exposing more inner aluminum for oxidation reactions. Subsequently, fluorinated segments produced by 2-NCF react with the alumina to form a β-AlF_3 layer, which rapidly transforms into a loose α-AlF_3 layer. Oxygen then permeates through the gaps in the α-AlF_3 layer to continue reacting with the inner aluminum, and the abundant gases generated cause the shell to fragment, releasing significant energy during the combustion process. Furthermore, 2-NCF significantly enhances the hydrophobicity of Al MPs, transforming the contact angles of pristine Al MPs from 0° to 120°. The long-term water resistance experiment further confirms that 2-NCF can effectively block water penetration and prevent hydrolysis of the inner aluminum. These results demonstrate that 2-NCF coated Al MPs exhibit excellent performance in ignition, combustion, and hydrophobicity due to the combination of fluorine content and high energy-containing properties of 2-NCF. This work may provide a new possibility for improving the combustion and storage performance of aluminum powder, a key component in propellants.

CRediT Authorship Contribution Statement

Tingting Ma: Writing – original draft, Investigation, Data curation. Junjian Xie: Formal analysis. Hui Li: Validation, Methodology. Kaixin Wei: Validation. Zhibin Xu: Resources. Zihui Meng: Supervision. Xiu-Tian-feng E: Writing – review & editing, Project administration, Funding acquisition, Formal analysis.

Declaration of Competing Interest

The authors declare that they have no known competing financial interests or personal relationships that could have appeared to influence the work reported in this paper.

Acknowledgements

This work was supported by the National Natural Science Foundation of China (22105024). The authors would like to acknowledge professor Shuo Wang from BIT for her supply of Al power.

Supplementary Material

Supplementary data to this article can be found online at https://doi.org/10.1016/j.cjche.2025.09.035.

References

[1] S.X. Sun, B.B. Zhao, G.P. Zhang, Y.J. Luo, Applying mechanically activated Al/PTFE in CMDB propellant, *Propellants Explos*, *Pyrotech* 43 (11) (2018) 1105–1114.
[2] N.H. Yen, L.Y. Wang, Reactive metals in explosives, *Propellants Explos*, *Pyrotech.* 37 (2) (2012) 143–155.
[3] C.C. Zeng, Z.J. Yang, Y.S. Wen, W. He, J.H. Zhang, J. Wang, C. Huang, F.Y. Gong, Performance optimization of core-shell HMX@(Al@GAP) aluminized explosives, *Chem. Eng. J.* 407 (2021) 126360.
[4] H.X. Wang, H. Ren, T. Yan, Y.R. Li, W.J. Zhao, A latent highly activity energetic fuel: thermal stability and interfacial reaction kinetics of selected fluoropolymer encapsulated sub-micron sized Al particles, *Sci. Rep.* 11 (1) (2021) 738.
[5] C. Wang, X.R. Zou, S.P. Yin, J.L. Wang, H.Y. Li, Y. Liu, N.F. Wang, B.L. Shi, Improvement of ignition and combustion performance of micro-aluminum particles by double-shell nickel-phosphorus alloy coating, *Chem. Eng. J.* 433 (2022) 133585.
[6] D.Y. Tang, J.Y. Lyu, W. He, J. Chen, G.C. Yang, P.J. Liu, Q.L. Yan, Metastable intermixed Core-shell Al@M(IO_3)$_x$ nanocomposites with improved combustion efficiency by using tannic acid as a functional interfacial layer, *Chem. Eng. J.* 384 (2020) 123369.
[7] F. Xiao, Z.H. Liu, T.X. Liang, R.J. Yang, J.M. Li, P. Luo, Establishing the interface layer on the aluminum surface through the self-assembly of tannic acid (TA): improving the ignition and combustion properties of aluminum, *Chem. Eng. J.* 420 (2021) 130523.
[8] Q.L. Qiu, Y.N. Zhou, J.Z. Liu, W. Shi, W.J. Yang, Combustion of aluminum powder using CO_2 laser in O_2/CO_2 atmosphere under different pressure conditions, *J. Therm. Anal. Calorim.* 147 (8) (2022) 4959–4970.
[9] Y.M. Huang, J.X. Zhang, R.H. Wang, B. Gao, R.Y. Miao, S.R. Zhang, D.J. Wang, Enhancing the energy release performance of Al@(1H, 1H, 2H, 2H-perfluorodecyltriethoxysilane/Glycidyl azide polymer) core-shell materials *via in situ* polymerization, *Colloids Surf. A Physicochem*, *Eng. Aspects* 710 (2025) 136278.
[10] Y.R. Li, H. Ren, T. Yan, Q.J. Jiao, H.X. Wang, Reactivity of fluororubber-modified aluminum in terms of heat transfer effect, *J. Therm. Anal. Calorim.* 142 (2) (2020) 871–876.
[11] J.Y. Piao, S.Y. Duan, Y.F. Mao, J. Wang, A.M. Cao, L. Zhang, Stabilization of the energetic Al powder through uniform and controlled surface coating for promoting its energy output, *Surf. Coat. Technol.* 389 (2020) 125603.
[12] L.T. DeLuca, Overview of Al-based nanoenergetic ingredients for solid rocket propulsion, *Def. Technol.* 14 (5) (2018) 357–365.
[13] J.F. Yuan, J.Z. Liu, Y.N. Zhou, J.R. Wang, T. Xv, Aluminum agglomeration of AP/HTPB composite propellant, *Acta Astronaut.* 156 (2019) 14–22.
[14] W. He, J.Y. Lyu, D.Y. Tang, G.Q. He, P.J. Liu, Q.L. Yan, Control the combustion behavior of solid propellants by using core-shell Al-based composites, *Combust. Flame* 221 (2020) 441–452.
[15] F. Saceleanu, T.V. Vuong, E.R. Master, J.Z. Wen, Tunable kinetics of nano-aluminum and microaluminum powders reacting with water to produce hydrogen, *Int. J. Energy Res. (2019) 4769.*
[16] F.W. Li, Q. Wang, J. Cheng, Z.H. Zhang, Y.X. Zhou, K.E. Ouyang, J.B. Xu, Y.H. Ye, R.Q. Shen, Mitigating the negative catalytic effect of CuO by FAS-17 coated Al nanopowder: isothermal ageing of Al/CuO nanotHermite at 71 °C and 60% relative humidity, *Def. Technol.* 34 (2024) 156–167.
[17] J.P. Liu, H.R. Zhang, Q.L. Yan, Anti-sintering behavior and combustion process of aluminum nano particles coated with PTFE: a molecular dynamics study, *Def. Technol.* 24 (2023) 46–57.
[18] Y.N. Li, S.Y. Hang, J. Li, W.X. Guo, W. Xiao, Z.W. Han, B.L. Wang, Study on the preparation parameters and combustion performance of Al/PTFE composites prepared by a mechanical activation-sintering method, *New J. Chem.* 44 (48) (2020) 21092–21099.
[19] J. Wang, L. Zhang, Y.F. Mao, F.Y. Gong, An effective way to enhance energy output and combustion characteristics of Al/PTFE, *Combust. Flame* 214 (2020) 419–425.
[20] Z.Y. Wu, J.X. Liu, S. Zhang, X.Q. Liu, X. Xu, W.Z. Ma, S.K. Li, C. He, Enhanced thermal- and impact-initiated reactions of PTFE/Al energetic materials through ultrasonic-assisted core-shell construction, *Def. Technol.* 18 (8) (2022) 1362–1368.
[21] H. Li, J.K. Zhang, F.Q. Zhao, X.F. Huang, Aluminum combustion enhancement in AP free nitramine- based solid propellants by PVDF coating, *Fuel* 390 (2025) 134689.
[22] Y.N. Li, B.L. Wang, Z.W. Han, Energy evolution mechanism of a PVDF activated nano-aluminum based metastable intermixed composites, *J. Alloys Compd.* 966 (2023) 171586.
[23] W.C. Zhang, K.Y. Xiong, Z.M. Fan, Y. Shu, P.J. Liu, Q.L. Yan, W. Ao, An experimental study of the combustion characteristics of novel Al/MO_X/PVDF metastable intermixed composites, *Aero. Sci. Technol.* 137 (2023) 108263.
[24] C.C. Wu, J.X. Nie, S.W. Li, W. Wang, Q. Pan, X.Y. Guo, Tuning the reactivity of perfluoropolyether-functionalized aluminum nanoparticles by the reaction interface fuel-oxidizer ratio, *Nanomaterials* 12 (3) (2022) 530.
[25] C.C. Wu, J.X. Nie, S.W. Li, Q.J. Jiao, D. Wang, X.Y. Guo, μAl-based reactive materials with improved energy efficiency by using the fluorine-containing oxidizer perfluoropolyether as an interfacial layer, *Combust. Flame* 248 (2023) 112554.
[26] L.C. Zhang, X.D. Li, S. Wang, X. Su, M.S. Zou, Facile energetic fluoride chemistryinduced organically coated aluminum powder with effectively improved ignition and combustion performances, *J. Therm. Anal. Calorim.* 148 (13) (2023) 5957–5966.
[27] H.X. Zhang, F. Xiao, Surface fluorinated metastable aluminum microspheres: improved ignition and anti-aging properties of aluminum powder, *Combust. Sci. Technol.* 197 (3) (2025) 618–635.
[28] L.L. Campbell, K.J. Hill, D.K. Smith, M.L. Pantoya, Thermal analysis of micro-scale aluminum particles coated with perfluorotetradecanoic (PFTD) acid, *J. Therm. Anal. Calorim.* 145 (2) (2021) 289–296.
[29] Y.H. Hu, B.W. Tao, D.Y. Hao, R.Q. Fan, D.B. Xia, K.F. Lin, A.M. Pang, Y.L. Yang, Fabrication and mechanistic study of AP/nAl/PTFE spherical encapsulated energetic materials with enhanced combustion performance, *Chem. Eng. Sci.* 222 (2020) 115701.
[30] Z.J. Li, X. Zhao, G. Li, F.Y. Gong, Y. Liu, Q.L. Yan, Z.J. Yang, F.D. Nie, Surface fluorination of *n*-Al particles with improved combustion performance and adjustable reaction kinetics, *Chem. Eng. J.* 425 (2021) 131619.

[31] R.B. Wang, L.C. Zhang, X.D. Li, L.X. Zhu, Z.L. Xiang, J. Xu, D.C. Xue, Z.T. Deng, X. Su, M.S. Zou, High-performance aluminum fuels induced by monolayer self-assembly of nano-sized energetic fluoride vesicles on the surface, *Adv. Sci.* 11 (26) (2024) 2401564.
[32] F. Xiao, T.X. Liang, Preparation of hierarchical core-shell Al-PTFE@TA and Al-PTFE@TA-Fe architecture for improving the combustion and ignition properties of aluminum, *Surf. Coat. Technol.* 412 (2021) 127073.
[33] Y. Chen, K. Xue, Y. Liu, L. Pan, X.W. Zhang, J.J. Zou, Preparation and properties of high-energy-density aluminum/boron-containing gelled fuels, *Chin. J. Chem. Eng.* 65 (2024) 230–242.
[34] V. Chobaomsup, M. Metzner, Y. Boonyongmaneerat, Superhydrophobic surface modification for corrosion protection of metals and alloys, *J. Coating Technol. Res.* 17 (3) (2020) 583–595.
[35] H.M. Ali, M.A. Qasim, S. Malik, G. Murtaza, Techniques for the fabrication of super-hydrophobic surfaces and their heat transfer applications. Heat Transfer - Models, Methods and Applications, InTech, 2018.
[36] L.C. Zhang, X.D. Li, S. Wang, X. Su, M.S. Zou, Self-assembly of composite salts induced uniform, ammonium perchlorate-catalytic, ignitable and energetic coating on aluminum fuels, *Combust. Flame* 260 (2024) 113109.
[37] Y. Pan, Y.J. Chen, K.L. Wu, Z. Chen, S.J. Liu, X. Cao, W.C. Cheong, T. Meng, J. Luo, L.R. Zheng, C.G. Liu, D.S. Wang, Q. Peng, J. Li, C. Chen, Regulating the coordination structure of single-atom Fe-N_xC_y catalytic sites for benzene oxidation, *Nat. Commun.* 10 (2019) 4290.
[38] K. Kamiya, H. Koshikawa, H. Kiuchi, Y. Harada, M. Oshima, K. Hashimoto, S. Nakanishi, Inside cover picture: Iron–nitrogen coordination in modified graphene catalyzes a four-electron-transfer oxygen reduction reaction, *Chemelectrochem* 1 (5) (2014) 820.
[39] M.A. Trunov, M. Schoenitz, X.Y. Zhu, E.L. Dreizin, Effect of polymorphic phase transformations in Al_2O_3 film on oxidation kinetics of aluminum powders, *Combust. Flame* 140 (4) (2005) 310–318.
[40] Z. Nie, H.F. Yang, M.H. Zhang, W.M. Wang, X.L. Fu, Z.Q. Qiao, G.C. Yang, X. Y. Liu, X. Wang, Synergistically enhanced long-term effectiveness and combustion performance of aluminum nanoparticles by partially fluorinating external alumina shell, *Ind. Eng. Chem. Res.* 61 (43) (2022) 16071–16080.
[41] M. Yang, D.Z. Gao, T. Wen, J. Guo, X.Q. Zhang, Q. Wang, C.P. Guo, Efficient construction of Al/F microspheres in pickering emulsion to regulate combustion reactivity, *J. Mater. Sci.* 59 (7) (2024) 2828–2840.
[42] Y. Chen, J.Q. Wang, Y.N. Wang, B.Z. Zhu, Y.L. Sun, Probing the difference in improving the ignition and combustion of micro/nano-sized aluminum powder modified by VitonA, *J. Mater. Sci.* 59 (48) (2024) 22091–22108.
[43] D. Riello, C. Zetterström, C. Parr, M.A.L. Braulio, M. Moreira, J.B. Gallo, V.C. Pandolfelli, AlF_3 reaction mechanism and its influence on α-Al_2O_3 mineralization, *Ceram. Int.* 42 (8) (2016) 9804–9814.
[44] C. Huang, Z.J. Yang, Y.C. Li, B.H. Zheng, Q.L. Yan, L.F. Guan, G. Luo, S.B. Li, F.D. Nie, Incorporation of high explosives into nano-aluminum based microspheres to improve reactivity, *Chem. Eng. J.* 383 (2020) 123110.
[45] B.Z. Zhu, S.Y. Zhang, Y.L. Sun, Y.W. Ji, J.H. Wang, Fluorinated graphene improving thermal reaction and combustion characteristics of nano-aluminum powder, *Thermochim. Acta* 705 (2021) 179038.
[46] E.L. Dreizin, Metal-based reactive nanomaterials, *Prog. Energy Combust. Sci.* 35 (2) (2009) 141–167.
[47] R.K. Walzel, V.I. Levitas, M.L. Pantoya, Aluminum particle reactivity as a function of alumina shell structure: amorphous versus crystalline, *Powder Technol.* 374 (2020) 33–39.
[48] V. Dichiarante, M.I. Martinez Espinoza, L. Gazzera, M. Vuckovac, M. Latikka, G. Cavallo, G. Raffaini, R. Oropesa-Nuñez, C. Canale, S. Dante, S. Marras, R. Carzino, M. Prato, R.H.A. Ras, P. Metrangolo, A short-chain multibranched perfluoroalkyl thiol for more sustainable hydrophobic coatings, *ACS Sustainable Chem. Eng.* 6 (8) (2018) 9734–9743.
[49] M. Abdolmaleki, G.R. Allahgholipour, H. Tahzibi, S. Azizian, Fabrication of superhydrophobic aluminum with enhanced anticorrosive property, *Mater. Chem. Phys.* 313 (2024) 128711.